Environmental Research 252 (2024) 118877

Contents lists available at ScienceDirect

Environmental Research

journal homepage: www.elsevier.com/locate/envres

Uranium contamination of bivalve *Mytilus galloprovincialis*, speciation and localization

Romain Stefanelli [a,b], Maria Rosa Beccia [a], Pier Lorenzo Solari [c], David Suhard [d], Sophie Pagnotta [e], Aurélie Jeanson [a], Jean Ulrich Mullot [f], Françoise Vernier [f], Christophe Moulin [b], Marguerite Monfort [b,**], Jean Aupiais [b,***], Christophe Den Auwer [a,*]

[a] Université Côte d'Azur, CNRS, Institut de Chimie de Nice, 06108 Nice, France
[b] CEA, DAM, DIF, F-91297 Arpajon, France
[c] Synchrotron Soleil, L'Orme des Merisiers, Saint-Aubin, BP 48, F-91192 Gif-sur-Yvette Cedex, France
[d] Institut de Radioprotection et de Sûreté Nucléaire (IRSN), PSE-SANTE/SESANE/LRSI, Fontenay-aux-Roses 92260, France
[e] Université Côte d'Azur, Centre Commun de Microscopie Appliquée, 06108 Nice France
[f] Toulon Naval Base, LASEM, BP 61, 83800 Toulon Cedex 9 France

ARTICLE INFO

Keywords:
Marine radioecology
Environmental radiochemistry
Uranium

ABSTRACT

Uranium is a natural radioelement (also a model for heavier actinides), but may be released through anthropogenic activities. In order to assess its environmental impact in a given ecosystem, such as the marine system, it is essential to understand its distribution and speciation, and also to quantify its bioaccumulation. Our objective was to improve our understanding of the transfer and accumulation of uranium in marine biota with mussels taken here as sentinel species because of their sedentary nature and ability to filter seawater.

We report here on the investigation of uranium accumulation, speciation, and localization in *Mytilus galloprovincialis* using a combination of several analytical (Inductively Coupled Plasma Mass Spectrometry, ICP-MS), spectroscopic (X ray Absorption Spectroscopy, XAS, Time Resolved Laser Induced Fluorescence Spectroscopy, TRLIFS), and imaging (Transmission Electron Microscopy, TEM, μ-XAS, Secondary Ion Mass Spectrometry, SIMS) techniques. Two cohorts of mussels from the Toulon Naval Base and the Villefranche-sur-Mer location were studied. The measurement of uranium Concentration Factor (CF) values show a clear trend in the organs of *M. galloprovincialis*: hepatopancreas ≫ gill > body ≥ mantle > foot. Although CF values for the entire mussel are comparable for TNB and VFM, hepatopancreas values show a significant increase in those from Toulon *versus* Villefranche-sur-Mer.

Two organs of interest were selected for further spectroscopic investigations: the byssus and the hepatopancreas. In both cases, U(VI) (uranyl) is accumulated in a diffuse pattern, most probably linked to protein complexing functions, with the absence of a condensed phase.

While such speciation studies on marine organisms can be challenging, they are an essential step for deciphering the impact of metallic radionuclides on the marine biota in the case of accidental release. Following our assumptions on uranyl speciation in both byssus and hepatopancreas, further steps will include the inventory and identification of the proteins or metabolites involved.

1. Introduction

Understanding the distribution, transfer, and bioaccumulation of anthropogenic metals in a given ecosystem is fundamental for assessing their environmental and biological impact on living species. Among these metals, radionuclides originating from human nuclear activities, in both regular operation and accidental release, are of specific concern because of their potential double chemical and radiological toxicity. Since the ramp up of the nuclear industry in the post WWII era, radionuclide discharges have been monitored in soil and aquatic

* Corresponding author.
** Corresponding author.
*** Corresponding author.
E-mail address: christophe.denauwer@univ-cotedazur.fr (C. Den Auwer).

https://doi.org/10.1016/j.envres.2024.118877
Received 29 January 2024; Received in revised form 2 April 2024; Accepted 3 April 2024
Available online 11 April 2024

environments (UNSCEAR, 2015). The objective of this study is part of our effort to improve our understanding of the transfer and accumulation of metallic radionuclides in the ecosystems. Our strategy is to define a model ecosystem at the laboratory scale that is a compromise between the environmental conditions and the limitations (detection limits) of the spectroscopic techniques.

So-called actinide elements have distinct characteristics: they are all radioactive regardless of isotopy and they can be bioaccumulated by living species, although they have no known essential role in any biological processes. In the actinide family, uranium (U) is a radioelement that occurs naturally in the environment and is used in the nuclear industrial cycle. Natural uranium (^{Nat}U) is a mixture of three different isotopes: uranium-238 (99.28% natural abundance), uranium-235 (0.71%) and uranium-234 (0.0054%). It is found in the earth's crust with an average concentration of 2.7 ppm in the form of various minerals (e.g. uraninite, autunite) (Eisenbud and Gesell, 1997; Lambert and Heier, 1968) although with large geographical heterogeneities. But uranium under various isotopes may also be released through anthropogenic activities such as atmospheric nuclear weapons testing (Sakaguchi et al., 2009; Winkler et al., 2012), nuclear fuel processing plants (Castrillejo et al., 2020), accidents (Lin et al., 2021; Sandalls et al., 1993) and mining activities (Beneš, 1999). Fossil fuels such as coal, as well as phosphate fertilizers widely used in agriculture, are also sources of ^{Nat}U dissemination that can contaminate terrestrial or marine compartments (UNSCEAR, 2015). In seawater, the ^{Nat}U concentration is averaged at 0.0033 ppm (13.8 nM), although differences occur from one body of water to another (Atwood, 2010; Morris and Raiswell, 2002). Because ^{Nat}U is easier to manipulate in the laboratory (low specific activity), it may be used as a chemical surrogate for heavier actinides (neptunium, plutonium), which are more difficult to manipulate, under specific (bio) chemical conditions. Uranyl $U(VI)O_2^{2+}$ for instance is worth studying as a chemical model for neptunyl $Np(V)O_2^{+}$ and plutonyl $Pu(V)O_2^{+}$ that can both occur in seawater (Topin and Aupiais, 2016).

The fate of trace metals in the environment is determined by their speciation (chemical and physical reactivity) and their transport (drifts, lixiviation, streams). Among all the compartments that are known as environmental repositories, seas and oceans can be considered as the final receptacle by the contribution of rivers and coastal erosion. In order to monitor marine contamination by metals, many international programs (Med Pol (UNEPMAP, 2023), OSPAR Convention (OSPAR, 2018), etc. have launched studies with living organisms such as mollusks and fish (*Mullus barbatus, Platichthys flesus, Zoarces viviparus, Perca fluviatilis, Pantala flavescens etc.)* used as sentinel species. Mollusks, especially mussels, are used to understand environmental pollution because of their ability to filter large volumes of seawater, their sedentary nature and the potentially harmful impact on human beings when consumed. (1,625,000 tons are consumed in the world each year) (Beyer et al., 2017; Liang et al., 2004; Rainbow, 1995; Widdows and Donkin, 1992). Two mussel species are widely used (*Mytilus edulis* and *Mytilus galloprovincialis*) as bio-indicators or biomarkers (Goldberg and Bertine, 2000; Jeng et al., 2000; Wang et al., 1996) in marine pollution monitoring programs such as the Mussel Watch Program (MWP) or the Mediterranean Mussel Watch (MMW) program (Carpene and George, 1981; Machado and Lopes-Lima, 2011; Wang and Fisher, 1999). The data from these programs can be used and compiled in the framework of national and international regulations. In the specific case of metallic radionuclides and environmental radioactivity monitoring, the International Atomic Energy Agency (IAEA) provides values of Concentration Factors (CF) for many radionuclides and several organisms (e.g. microalgae, mussels, fish, octopus). The interaction of radionuclides with marine biota (IAEA, 1973) was described as early as 1972 at one of the first IAEA symposia on the marine environment. These data are not only relevant for comprehending oceanographic processes but for ensuring the availability of dependable data on element concentrations in seawater as well. The CFs are expressed according to the concentration of an element in a biological sample over the concentration of the element in the ambient seawater in dry or wet weight. Concentration Factors, CFs, were calculated using the following formula (1) (dimensionless):

$$CF = \frac{Concentration\ per\ unit\ mass\ of\ the\ organism/organs\ (kg/kg)}{Concentration\ per\ unit\ mass\ of\ seawater\ (kg/kg)} \quad (1)$$

In the aquatic environment, uranium is found in two forms: tetravalent U(IV) mainly in immobile colloidal forms and hexavalent U(VI) that is a more soluble form known as uranyl UO_2^{2+}. The uranyl form is ubiquitous in atmospheric conditions unless a specific reducing mechanism is activated. This is also the case in seawater where speciation studies have confirmed the occurrence of the uranyl tricarbonato complex (Gascoyne, 1992; Konstantinou and Pashalidis, 2004; Maloubier et al., 2015). Because the chemical toxicity of ^{Nat}U is higher than its radiotoxicity, its potential effects on biota are essentially considered similar to those of a heavy metal. There have been several laboratory studies examining uranium uptake and toxicity in various aquatic organisms including both fish and invertebrates (Beyer et al., 2017; Rainbow, 1995). In marine organisms, uranium shows low CFs of the order of a few tens of units due to the absence of biological processes associated with this element, while essential metals such as Fe and Zn have typical CFs of the order of 10^3 - 10^5. For example, in mollusks, Fe has a recommended CF value of 5.10^5 (Beyer et al., 2017; Rainbow, 1995).

The mussels considered in this work are ideal candidates as bioindicators because of their great numbers, their ubiquitous distribution, their facility of being collected in large quantities and their resilience to laboratory experiments for *in vivo* studies. Reported studies performed with mollusks have revealed three different ways in which heavy metals may accumulate. The first is accumulation by passive diffusion of water-soluble species. In fact, several studies have shown the importance of the gills in the internalization of cadmium (Carpene and George, 1981; Machado and Lopes-Lima, 2011; Wang and Fisher, 1999). Second, heavy metals can be actively accumulated via transmembrane ion-pump transport. In *M. galloprovincialis*, the Ca^{2+} channels can facilitate the entry into the cells of Cd^{2+} ions via Ca-dependent pumps (Li et al., 2015; Viarengo and Nott, 1993; Viarengo et al., 1999). Finally, the phenomena of endocytosis of particles present in water can participate in the bioaccumulation process. These phenomena occur specifically in the gut and can cause tissue damage (Simon et al., 2011). Moreover, a fraction of accumulated heavy metals can be stored in a non-toxic form in the cells influenced by the bioavailability of the metal in the organism (Kägi and Kojima, 1987). Among the various organs, the hepatopancreas is known to be a storage site for heavy metal accumulation (Markich, 1998). The bioaccumulation of some metals such as Cd, Ni, Cr, Pb, and Hg can cause oxidative stress and the generation of reactive oxygen species in tissues when their concentrations become excessive (Li et al., 2015; Viarengo and Nott, 1993; Viarengo et al., 1999). In addition, these metals can have a direct impact on the activity of certain proteins: for instance, metallothionein are low molecular weight cytosolic proteins rich in SH groups that demonstrate a high degree of upregulation when metal concentrations in the environment increase (Marigómez et al., 2002; Markich, 1998).

Yet another mechanism of metal storage could involve the secretion of byssal threads in which metals are concentrated. This thread is an inert organ that allows mussels to anchor to their support. Proteins present in the byssus and their possible complexation sites have been well characterized and are predominantly distributed in the protective cuticle (e.g., "mussel foot protein") and in the fibrous, collagen-rich core (Harrington et al., 2018; McCartney, 2021; Torres et al., 2012).

The objective of this study was to improve our understanding of the bioaccumulation of uranium in mussel *Mytilus galloprovincialis* taken here as model species. To this end, we used a combination of analytical and spectroscopic techniques to describe the chemical speciation and localization of uranium (uranyl) following accumulation in

M. galloprovincialis. We excluded from this study the effects of radiation because the specific activity of natural uranium is very low (25,570 Bq. g^{-1}). To our knowledge, quantification of accumulation, techniques such as imaging and chemical speciation investigation are rarely combined in radioecological studies. While they can be challenging, speciation studies on living marine organisms are also an essential step for deciphering the impact of metallic radionuclides on the marine biota. But at this stage, the biochemical and biological assessment of the accumulation is beyond the scope of this article.

2. Materials and methods

Inductively Coupled Plasma Mass Spectrometry (ICP-MS), was used to determine the CF, quantify the distribution of uranium in various organs, namely the hepatopancreas, gills, visceral mass, mantle, foot and byssus as well as in the subcellular compartments. Micro X-ray Fluorescence imaging (μ-XRF), Transmission Electron Microscopy (TEM) and Secondary Ion Mass Spectrometry (SIMS) images provided information on uranium distribution at different scales from the organ scale to the subcellular scale. Two X-ray Absorption Spectroscopic (XAS) modes were used to decipher the speciation of uranium in the organs in question: i) bulk XAS with Extended X-ray Absorption Fine Structure (EXAFS) and X-ray Absorption Near Edge Structure (XANES); ii) and μ-XANES. Speciation was also enhanced by employing Time-Resolved Laser-Induced Fluorescence Spectroscopy (TRLIFS). This method allows for the investigation of low uranium concentrations (10^{-9} M) and provides robust results in terms of fluorescence emission and fluorescence lifetime (Moulin et al., 1998).

2.1. Seawater, mussel collection, and aquarium setup

Seawater was collected in the Mediterranean Sea at Villefranche-sur-Mer, by the Laboratoire Océanographique de Villefranche at 50 m from the shore of Villefranche-sur-Mer, 5 m deep (43°41′44.4″N 7°18′28.0″E). The seawater was pre-filtered at 1 μm (Crystal filter (PP-01-978)). *M. galloprovincialis* were collected near the coast of Saint-Jean-Cap-Ferrat (43°41′02.4″N 7°18′56.2″E) (June 2021) by the service "Moyen à la Mer" of the Laboratoire Océanographique de Villefranche-sur-Mer (FR3761, Mediterranean Sea, France) and in an area inside the Toulon Naval Base (43°06.3445 N, 05°54.6119 E) (February 2022) by naval military divers (Supplementary Fig. S1- SI). In the laboratory, mussels were maintained in 30 L seawater glass tanks (40 × 26 × 30 cm LxWxH) during the experiments. The seawater temperature was maintained at 16–17 °C using a water-cooling system. Mussels were fed with *Isochrysis galbana* (purchased at CCAP) with 10^4 cell/mussel every 3 days. Before contamination, mussels were left for an adaptation period of 3 days. The seawater was changed after 7 days.

Mussels from Villefranche-sur-Mer (VFM) and Toulon Naval Base (TNB) were divided into two groups of 82 and 79 individuals, respectively. Seawater was doped with one spike at t = 0 with [U(VI)] = 6.10^{-7} M, renewed after t = 7 days and spiked in the same contamination conditions. After contamination, for VFM and TNB cohorts, the first group with average length 6.5 cm ± 0.5 cm was dissected, and organs were separated (foot, gill, byssus, mantle, hepatopancreas, and the rest of the body). The second group with a length between 6.5 and 2.5 cm was dissected, and the fleshy part was kept whole (the size distribution of the cohorts is illustrated in Fig. S2, and the organs studied in Fig. S3 of SI).

Replicate experiments were performed with the *M. galloprovincialis* from VFM but focused solely on speciation and performing X-ray and laser spectroscopies. Four different glass aquaria (19 × 19 × 25 cm; LxWxH) were used during the experiments. Each aquarium contained 2 mussels placed into 2 L of doped seawater with uranium. A series of contaminations were carried out with varying concentrations of uranium, adjusted according to the detection limit of spectroscopic methods. The concentrations used were kept as low as possible in order to approximate environmental levels (Table S1 of SI).

Ex vivo sorption experiments of the byssal thread were performed from freshly cut byssus of uncontaminated mussels as described in section III of SI. Byssus were immersed for 14 days in uranium-doped seawater ([U] = 10^{-3} M).

Uranium quantification and concentration factors determination is described in section III of SI together with statistical analysis.

2.2. Subcellular fractionation

Subcellular fractionations were performed with protocols described by Wallace and Luoma (2003) and adapted for this work (see section III and Fig. S4 of SI).

2.3. Transmission electron microscopy (TEM) imaging

Organs were fixed in 2.5 % glutaraldehyde for 24 h at 4 °C. After rinsing with distilled water, they were dehydrated through an increasing ethanol series and embedded in epoxy resin. The ethanol solutions were analyzed by ICP-MS and do not contain traces of uranium. Ultrathin sections (70 nm) were cut using a diamond mounted on an ultramicrotome (Ultracut S, Leica) and placed on copper TEM grids coated and examined with a JEOL JEM 1400 TEM equipped with a CCD camera (Morada, Olympus SIS) at the Centre for Applied Microscopy (CCMA, University of Nice Sophia Antipolis, Nice, France).

2.4. Time-Resolved Laser-Induced Fluorescence Spectroscopy (TRLIFS)

Sample preparation for TRLIFS: Hepatopancreas samples were homogenized with Potter-Elverhjem glass with Teflon pestle at 4 °C and 10 sonication cycles (High; 30s ON/OFF) in an ice bath. The homogenate was stored at 4 °C until analysis the following day.

Data acquisition: A Nd:YAG laser (Model Surelite Quantel) operating at 355 nm (tripled) and delivering about 10 mJ of energy in a 10 ns pulse with a repetition rate of 10 Hz, was used as the excitation source for uranium. The laser output energy was monitored by a laser power meter (Scientech). The focused output beam was directed onto the sample placed in a 0.35 mL quartz cell of the spectrofluorometer (F920 Edinburgh). The detection was provided by an intensified charge coupled device (Andor Technology) cooled by Peltier effect (−20 °C) and positioned at the polychromator exit for the emission spectra measurement and by a photomultiplier tube (PMT) to measure the fluorescence decay time. Logic circuits, synchronized with the laser shot beam, allowed the intensifier to be activated with determined time delay (from 0.005 to 1000 μs) and during a determined aperture time (from 0.005 to 1000 μs). Data acquisition was performed using the F900 software (Edinburgh Instruments). From a spectroscopic point of view, various gate delays and duration were used to distinguish the presence of only one complex by the measurement of a single fluorescence lifetime and spectrum. Fluorescence lifetime measurements were performed by varying the temporal delay with fixed gate width. A reference solution of U(VI) for TRLIF measurements was obtained from a dilution of a standard solution of uranium (VI) (100 mg L−1 in H3PO4 0.1 M). Experimental data were analyzed using the software Origin (Pro), Version 2019.

2.5. X-ray Absorption Spectroscopy (XAS), extended X-ray absorption fine structure (EXAFS) and μ-X ray fluorescence mapping (μ-XRF)

2.5.1. Sample preparation

After dissection, the hepatopancreas samples were partially dried with KIMTECH tissue to remove excess water. Samples were homogenized in a mortar to obtain a wet powder mixed with polyethylene. Byssus was freeze-dried for 24 h and were homogenized in a mortar to obtain a powder mixed with polyethylene, thereby forming pellets which were then kept at 4 °C until analysis in order to limit any deterioration of the biological system. To overcome the analytical detection

limit of the synchrotron and laser probes, the contamination concentrations were increased to [U] = 5.10^{-5} M (see the Materials and Methods section). This range of concentration is at the lowest limit for obtaining an exploitable signal-to-noise ratio.

2.5.2. Sample preparation and μ-XRF mapping

The protocol is similar to that used for TEM with the resin embedding, with drying times extended to several days for entire mussels. Samples were cut with MECATOME T205 PRESI to obtain slices of 1–2 mm thickness.

2.5.3. Data acquisition

XAS and μ-XRF measurements were performed on the MARS beamline of the SOLEIL synchrotron facility. The MARS beamline is dedicated to the investigation of radioactive materials in the hard X-ray range and our radioactive samples must necessarily be analyzed on a dedicated beamline (Lorens et al., 2014; Sitaud et al., 2012). The main optics of the beamline consist essentially of a water-cooled double-crystal monochromator (FMB Oxford) which is used to select the incident energy of the X-ray beam. For horizontal focusing, and two large water-cooled reflecting mirrors (IRELEC/SESO) that are used for high-energy rejection (harmonic part) and vertical collimation and focusing. The measurements were performed in fluorescence mode close to the uranium L_{II} edge at 20,948 eV, to collect the ray $L_{\beta 1}$ of the uranium fluorescence line and to avoid the Sr K_{α} fluorescence. This choice was motivated by the presence of strontium in the mussels. The proximity of the fluorescence lines $K_{\alpha 1}$ and $K_{\alpha 2}$ of strontium to the L_{α} line of uranium at the L_{III} threshold would not have allowed for their distinction in the fluorescence spectra. The monochromator was set with Si(220) crystals and the mirrors were set with Pt reflecting stripes at an angle of 2.7 mrad. The fluorescence signal was collected using a 13-element high-purity germanium detector (ORTEC). Energy calibration was performed at the Molybdenum K edge at 20,000 eV. X-ray absorption spectra for all samples were measured at room temperature. The EXAFS spectra were recorded up to 13 $Å^{-1}$ with steps of 0.005 $Å^{-1}$ in the EXAFS regime, and each scan had a total integration time of approximately 50 min. XANES spectra on bulk were recorded with steps of 0.80 eV at the edge. XANES spectra on mapped samples were recorded with steps of 1.60 eV at the edge. The XANES spectra correspond to the average of two scans. The scan accumulation demonstrated stability in the spectra, with no observed photo-reduction during the analyses.

To reduce the beam size for μ-XRF cartography, additional Kirkpatrick–Baez (KB) mirrors were inserted in the beam. These consisted of rhodium coated trapezoidal mirrors (ZEISS) positioned at an angle of 2.5 mrad. The final beam size in this case was H × V: 29 × 24 μm^2 (FWHM). The mechanical parameters (with the mirrors set to optimize the flux at high energy) of the beamline do not allow for a beam size smaller than 1 μm at this energy. μ-XRF images were also obtained at the uranium L_{II} edge on the MARS and μ-XRF images were analyzed with software PyMCA (Solé et al., 2007). μ-XRF is based on the emission of X-ray fluorescence following the excitation of a core electron. This fluorescence emission is then selected to build 2D maps. The presence of double confinement (Kapton film) and resin attenuates the fluorescence of low-energy elements such as Ca and Na does not allow for the observation of specific structures. No artifacts related to the preparation of biological samples were detected during the mappings.

The treatment for embedded samples in resin did not reveal any diffusion of elements such as Ca, Na, Fe into the subcellular structures or the resin (SIMS imaging of hepatopancreas not shown). However, uranium speciation could change during the chemical treatment, which is why bulk samples without chemical treatment were also analyzed to preserve this chemical form.

EXAFS data fitting is described in section IV of SI.

2.6. SIMS microscopy

Sample preparation for SIMS:

Organs were fixed in 2.5% glutaraldehyde for 24 h at 4 °C. After rinsing with distilled water, they were then dehydrated through an increasing ethanol series and embedded in epoxy resin.

In SIMS, a high-energy primary ion beam strikes the surface and causes the ejection and ionization of secondary ions from the sample surface. To generate an ion 2D image, the focused primary ion beam scans the sample surface, providing visualization of the molecular distribution beneath the sample surface. The SIMS analysis was performed on an SIMS 7 F-E7 instrument (Cameca, France). For this study O^{2+} beam bombardment was used to enhance the ionization field of electropositive species such as uranium and the other major elements (Ca^{+}, Na^{+}) allowing structural representation. Analysis was carried out with a 5 nA, O^{2+} beam bombardment of 150 μm^2 and 200 μm^2 were used to acquire areas of interest. The collected secondary ions can be measured, and mass filtered with an electron multiplier and sequentially converted into an image. Mass resolution can reach M/ΔM = 10.000, where M is the molecular mass of the detected ion. For this experiment a M = 400 mass resolution was used. The lateral resolution (probe size) during this study is approximately 1.5 μm. The experimental conditions for this work and integration time of the different images are summarized in Table S2. For each area analyzed, mass spectra at around the mass of isotope 238 of uranium, and ion images were obtained. $^{23}Na^{+}$ and $^{40}Ca^{+}$ images give the histological structure of the organs and $^{238}U^{+}$ images show uranium fixation within the structures. The analyzed region is a 150 μm^2 raster, 100 plans are combined (added up) to form the byssus images and 200 plans for the hepatopancreas images.

3. Results

3.1. Uranium uptake by M. galloprovincialis and subcellular partitioning

A controlled marine system with living mussels was put in place and a contamination sequence was defined (see the Materials and Methods section). To be as close as possible to incidental contamination conditions with dispersion in oceanic media, the selected experimental concentration was a compromise of environmental trace levels (between *ca.* 10^{-8} and 10^{-6} M) and spectroscopically detectable levels.

Two cohorts of mussels from Villefranche-sur-Mer (VFM), which is considered unpolluted, and Toulon Naval Base (TNB), known to be polluted by heavy metals. The dissection procedures and uranium quantification are described in SI. CF values for each specimen of VFM and TNB are presented in Fig. S5 of SI. It was observed, after 12 days of contamination, that the average CF values for mussels ranging between 6.0 and 3.5 cm are equal to 15 and 16 for VFM and TNB, respectively. These values are consistent with the reported CF value (CF = 30) for uranium and mollusks reported in an IAEA report (IAEA, 2004). Note, however, that large variations are expected for different species within the same family. The presence of 3 juvenile mussels between 3.5 and 2.5 cm suggests that the accumulation kinetics of uranium appear to be different. However, a larger-scale study has not been conducted to confirm the differences between adult mussels and juvenile mussels. In the clam species *Gafrarium tumidum,* however, Heduoin et al. reported an inversely proportional relationship between size and CFs for some elements such as Cr, Cd, Co, and Zn (Hédouin et al., 2006).

Fig. 1 shows the CF values for each organ of the dissected mussel of the cohort (VFM and TNB). A significant difference between the hepatopancreas and the other organs can be observed. This trend follows the same pattern as transition metals such as Cd and Zn (Fisher et al., 1996; Li et al., 2015). The overall trend in CF distribution under the present experimental conditions follows the order: hepatopancreas ≫ gill > body ≥ mantle > foot. It has been verified that the sum of the amount of uranium in each organ is comparable to the amount in the entire mussel, indicating that there is no significant loss of material during the process

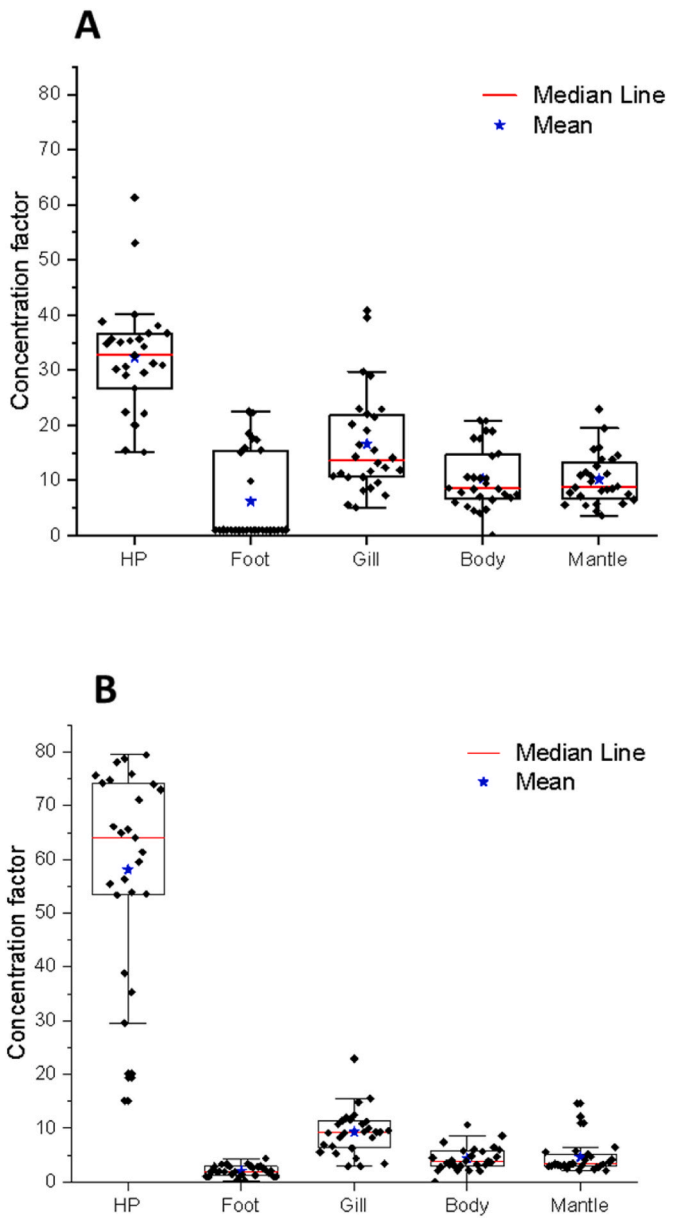

Fig. 1. Concentration factor of uranium in the five different organs from two different sampling stations: Villefranche-sur-Mer (A) Toulon Naval Base (B) (HP: hepatopancreas).

of analysis: TNB 2.3 ± 0.7 μgU.g^{-1} (dw) and VFM 3.4 ± 1.7 μgU.g^{-1} (dw) (dry weight of organs, excluding mussel sizes below 3.5 cm). An order of magnitude in absolute mass of U is (VFM values): 1.7 10^{-3} g of U in the aquarium (12 L total), 7 10^{-8} g in byssus, 4 10^{-8} g in hepatopancreas, 5 10^{-8} g in gills, keeping in mind that all organs have different masses. The main feature shared between the two cohorts is the significantly higher CF values observed in the hepatopancreas of the TNB mussels, compared to that of the VFM mussels (a factor of 2). The overall CF values of the gills, body, and mantle are lower for TNB than for VFM specimens. This significant difference could be attributed to environmental differences, as will be discussed in the last section. To quantify uranium in the byssal material accurately, the pre-existing byssus was cut off from the mussels along the shell before the experiment, and the fresh byssus created by the individual was analyzed at the end of the experiment. Quantification of the byssal material of mussels harvested at VFM shows widely scattered data shown in Fig. S6 of SI.

In addition to the evaluation of CFs, an investigation of uranium distribution within the subcellular compartments of the soft portions was performed, to better understand the mechanisms associated with its storage. For mollusks, metallothionein and metal-rich granules are recognized as leading the detoxification processes (Amiard et al., 2006; G. W. Bryan et al., 1979; Klerks and Bartholomew, 1991; Viarengo and Nott, 1993). The subcellular distribution of uranium in mussels after 12 days of accumulation (see the Materials and Methods section) was measured. It follows the order: enzymes (64%) > organelles (28%) > cellular debris (CD) (8%) > metal-rich granules (MRG) (1%) (Fig. S7 of SI). The enzyme fraction itself is divided into two sub-fractions: one containing thermo-sensitive proteins (28%) and the other comprising thermostable proteins (36%). Uranium is predominantly present in the cytosol of organelles (28%) and enzymes (64%) but is also significantly associated with compartments involved in detoxification pathways (MRG (1%) + thermostable protein (36%)).

3.2. *Byssus*

Byssus is a composite biomaterial that has attracted much interest because of its mechanical properties. The byssus is composed mainly of collagen that is directly connected to the soft tissue of the mussel. Byssal threads are produced by mussels and enable them to anchor firmly to a substrate (rocks). A drawing of the byssus structure can be seen in Fig. 2 for reference during this discussion. Two contamination procedures were implemented to obtain information on uranium accumulation. *In vivo* contamination is characterized by the mussel producing a byssus thread during uranium exposition, while *ex vivo* contamination involves exposing byssus threads to a seawater solution doped with uranium.

In vivo contamination: To localize the uranium contamination at the scale of the byssus filaments after *in vivo* contamination, X-ray fluorescence data were recorded in mapping mode at the L_{II} edge of uranium (see the Materials and Methods section). The μ-XRF images were superimposed with the optical images of the areas of interest to observe the distribution of uranium. As explained previously, the current beam line optics for μ -XRF do not allow us to achieve a beam size smaller than 20 μm. The entire byssus (Fig. 3A) shows an intense fluorescence of uranium in agreement with the large, but scattered, values of CFs. The byssus is composed of a central part called the byssus stem surrounded by byssus threads (Fig. 2). In the optical image, one can see the byssus stem and the byssus threads, which are also visible on the X-ray fluorescence map of uranium (Fig. 3B). At this scale, uranium is homogeneously localized on the byssal threads. The XANES spectra of the byssal threads and byssus stem were further compared to that of a Liebigite reference ($Ca_2UO_2(CO_3)_3$) because liebigite is a solid-state uranyl tricarbonate compound in which the uranyl cation has an environment comparable to seawater (Fig. S8 A and B of SI) (Maloubier et al., 2015). The XANES spectra recorded on various regions of the byssus consistently reveal strong similarities with a typical shoulder at *c. a.* 15 eV from the white line, indicative of the uranyl transdioxo multiple scattering feature (keeping in mind that the XANES of uranyl at the $L_{II, III}$ edges is not very structure sensitive). Therefore, the presence of uranyl (VI) species is confirmed, and no reduction to U(IV) occurs. Unfortunately, no useable EXAFS data could be recorded on those samples (with *in vivo* contamination) because of the very low signal-to-noise ratio collected at the edge (Fig. S9 of SI). In parallel, samples were also analyzed using transmission electron microscopy (TEM, Fig. S10 of SI), and secondary ion mass spectrometry (SIMS, Fig. 4). The SIMS images allow us to access a beam size that is compatible with the observation of substructures, which are impossible to obtain under the optical conditions we used in μ-XRF. No visible occurrence of U-precipitates (uranium condensed phases) appears in the byssus images either with TEM, with SIMS, or with μ-XRF (at respective resolutions). In addition to μ -XRF and TEM, SIMS analyses carried out show the presence of uranium in the core of the byssus threads (Fig. 4). These results are complementary to TEM, as ionic images can detect the presence of uranium even in non-condensed forms, providing spatial information. Considering the

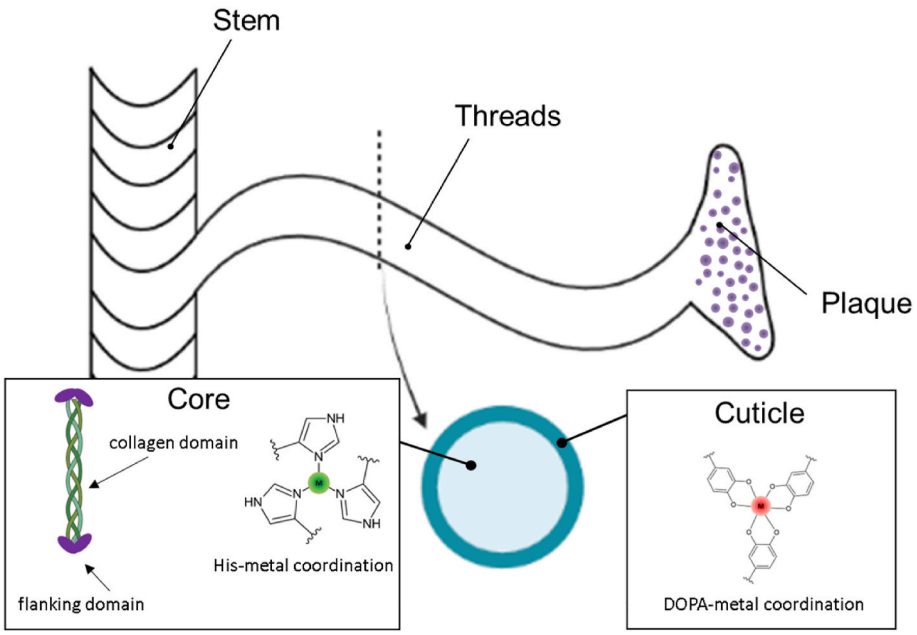

Fig. 2. Schematic representation of a byssal thread attached to the stem and terminated on the other side by a DOPA-containing, mussel foot protein (mfp) adhesive plate. The cuticle is the protective part of the thread and provides its strength, composed of proteins rich in DOPA motifs such as mfp-1. The core is formed by a repeating pattern of collagen and histidine-rich terminal parts.

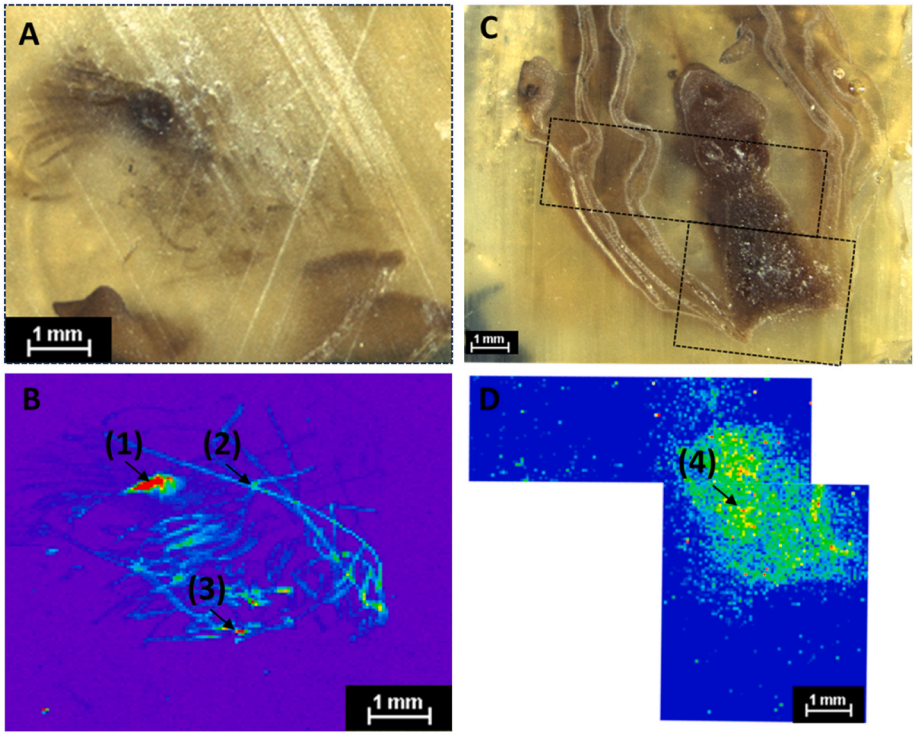

Fig. 3. Optic image of byssus (*in vivo*) (A) and X-ray fluorescence (uranium L_{II} edge) mapping of the byssus (B) (50 μm step size, 1.5 s integration time). Optic image of hepatopancreas (C) and X-ray fluorescence (uranium L_{II} edge) mapping of the hepatopancreas (50 μm step size, 1.5 s integration time). Mussels were contaminated in doped seawater with [U] = 5.10^{-5} M. The dotted areas show the fluorescence analysis zones and arrows indicate the areas where XANES have been performed. Scale bars represent 1 mm.

high CF values measured for this organ, one may consider that uranium is homogeneously stored in the byssus matrix and not precipitated as an inorganic condensed phase (e.g., uranyl-phosphate dense phase).

Ex vivo contamination: A second set of experiments was performed with byssus samples, collected fresh and contaminated *ex vivo* (see the Materials and Methods section)n. The fibrous matrix of the byssus is mainly made up of collagen fibers (Harrington et al., 2018; Hennebicq et al., 2013; McCartney, 2021). Proteins such as those found in the "mussel foot protein" family (mfps) containing catecholamine ligand motifs are also present in the byssal thread and plate. As described in Fig. 2, dihydroxyphenylalanine (DOPA) ligands, contained in mfps, are important metal chelating motifs that have also garnered interest due to

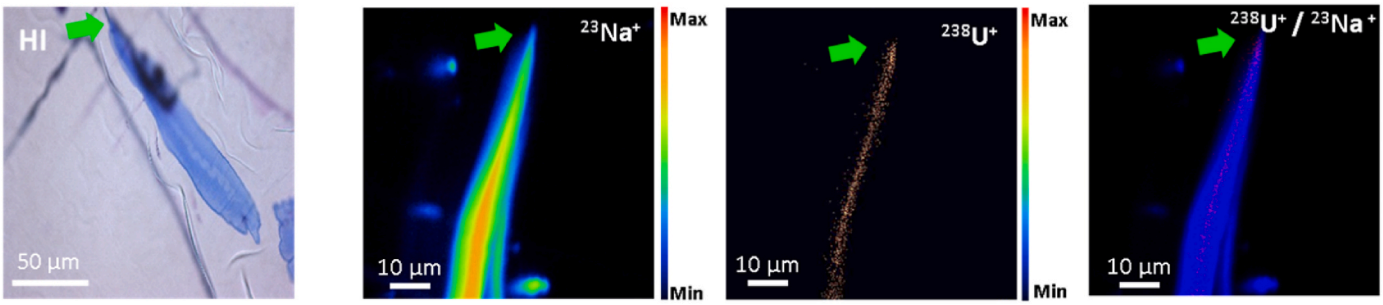

Fig. 4. HI: histological image of the byssus (*in vivo* contamination). Ionic (SIMS) images of $^{23}Na^+$, $^{238}U^+$ and overlay $^{238}U^+/^{23}Na+$of byssus produced by *M. galloprovincialis* during 12 days contamination experiments in doped in sea water with [U] = 5.10^{-5} M. Green arrows help to identify byssus.

their ability to allow the extraction of actinides, especially uranium, in aqueous media (Abney et al., 2017; Gorden et al., 2003; Mossand et al., 2023; Wu et al., 2017). There are several examples in the literature of uranyl-chelating molecules based on a 3,4-dihydroxyphenyl motif (Szigethy and Raymond, 2011). There is however no crystallographic information on uranyl-protein complexes containing 3,4-dihydroxyphenyl motifs. The EXAFS spectrum of the bulk sample, shown as the average of 4 scans (Fig. 5) and recorded at the U L_{II} edge, was adjusted using the best-fit structural parameters reported in Table 1. The best hypothesis is a coordination sphere made of 2 (fixed) U-O_{ax} bonds at a typical distance of 1.80 Å, 5 (1) U-O_{eq} bonds averaged at 2.45 Å and 5 (1) (linked) C located at 3.5 Å (typical of –CO ligation). The addition of the C path significantly improves both the quality factor and agreement factor of the fit (Q = 66, R = 1.5% *versus* Q = 39, R = 0.7%). The distances obtained from our adjustment are very comparable to the U-O_{eq} (2.40 Å) in the crystal structures of UO_2 $[TAM(HOPO)_2]\}^{2-}$ complex, for instance, very similar to the DOPA motif (Szigethy and Raymond, 2011).

Byssal thread samples were also analyzed by SIMS imaging (Fig. 6) to obtain information on the distribution of uranium after *ex vivo* contamination (to be compared with SIMS performed on byssus samples contaminated *in vivo*).). The SIMS images reveal the distribution of uranium, forming a thin layer of a few micrometers (≈5 µm) around the byssal threads. Correlation with the optical images indicates that uranium is localized at the level of the protective cuticle (5–10 µm thick). The sodium ion image of Fig. 6 allows us to distinguish between the protective cuticle of the byssus and the fibrous core. It also suggests the diffusion of uranium from the cuticle to the matrix of the threads, suggesting the migration of a soluble form of uranyl. This is also in agreement with the observation of Fig. 4 for which uranium from *in vivo* contamination is distributed inside the thread core. Finally, the presence of uranium on the protective cuticle is consistent with the data obtained from the EXAFS analysis. This part of the byssal thread is rich in proteins containing 3,4-dihydroxyphenylalanine (DOPA) motifs which was used to fit our experimental EXAFS data. This data clearly defines the protective cuticle as a target for uranium sorption.

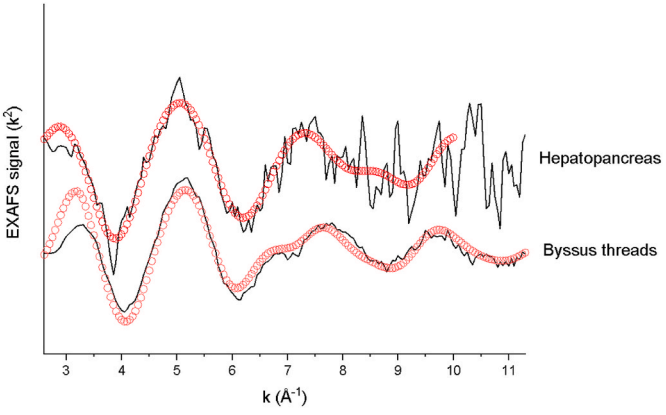

Fig. 5. EXAFS spectra (k^2) at the uranium L_{II} edge of the contaminated byssus threads (*ex vivo*) and hepatopancreas. Experimental = straight line; fit = red dots.

Table 1
Best Fit Parameters for EXAFS data collected at the uranium L_{II} edge.[a].

Organ	First coordination shell	Second coordination shell	Third coordination shell	Fit parameters[a]
Byssus threads	2 (fixed) O_{ax} at 1.80 (2) Å $\sigma^2 = 0.003$	5 (1) O_{eq} at 2.45 (5) Å $\sigma^2 = 0.013$ Å^2	5 (1) (linked) C at 3.5 (3) Å $\sigma^2 = 0.012$ Å^2	$S_0^2 = 1.1$ $e_0 = 5.53$eV $R_{factor} = 0.7$ %
Hepatopancreas	2 (fixed) O_{ax} at 1.75 (2) Å $\sigma^2 = 0.002$ Å^2	*4* (fixed) O_{eq} at 2.31 (3) Å $\sigma^2 = 0.006$ Å^2	*2* (fixed) S at 2.83 (10) Å $\sigma^2 = 0.011$ Å^2	$S_0^2 = 1.1$ $e_0 = -3.08$ eV $R_{factor} = 1.0$ %

[a] Numbers in brackets are the estimated uncertainties on the last digit. $\sigma^2$is the Debye Waller factor of the considered scattering path. $S_0^2$is the global amplitude factor, e_0 is the energy threshold, R_{factor} is the agreement factor of the fit in %.

3.3. Hepatopancreas

Fig. 3C shows the area corresponding to the hepatopancreas where the localization of uranium in this organ can be unambiguously observed. In Fig. 3D, within µ-XRF beam resolution of 29 × 29 µm, it is clearly visible that uranium is localized within the organ itself. The presence of uranium is confirmed by XANES spectra (Fig. S8A of SI) recorded inside the hepatopancreas while no signal was obtained outside. Note that several spectra recorded at different points within the hepatopancreas zone exhibit the same features, suggesting that the uranium speciation is homogeneous in this zone. The typical feature of uranyl (UO_2^{2+}) is observed after the white line with the presence of the transdioxo multiple scattering features, as in the case of byssus. This is a clear indication that there is no reduction to U(IV) in the hepatopancreas. This also demonstrates the organ-specific accumulation of uranium within the detection limit of the probe. TEM images (not provided) of the hepatopancreas contaminated in the same conditions do not show any specific, dense features due to uranium. This suggests that no condensed phase of uranium is present in the organ, thus confirming the observation with µ-XRF images.

To better understand the mechanisms of uranium uptake in *M. galloprovincialis*, EXAFS and Time-Resolved Laser-Induced Fluorescence Spectroscopy (TRLIFS) were combined. The EXAFS spectrum of the bulk sample is presented in Fig. 5 with a relatively low signal-to-noise ratio (average of 5 scans). Qualitative differences that are visible between the EXAFS spectra of the hepatopancreas and the byssus indicate probable differences in uranium speciation. The EXAFS spectrum of the hepatopancreas was tentatively adjusted with 3 types of oxygens + hetero-atoms: oxygens + carbons (O + C) that mimic carboxylates or

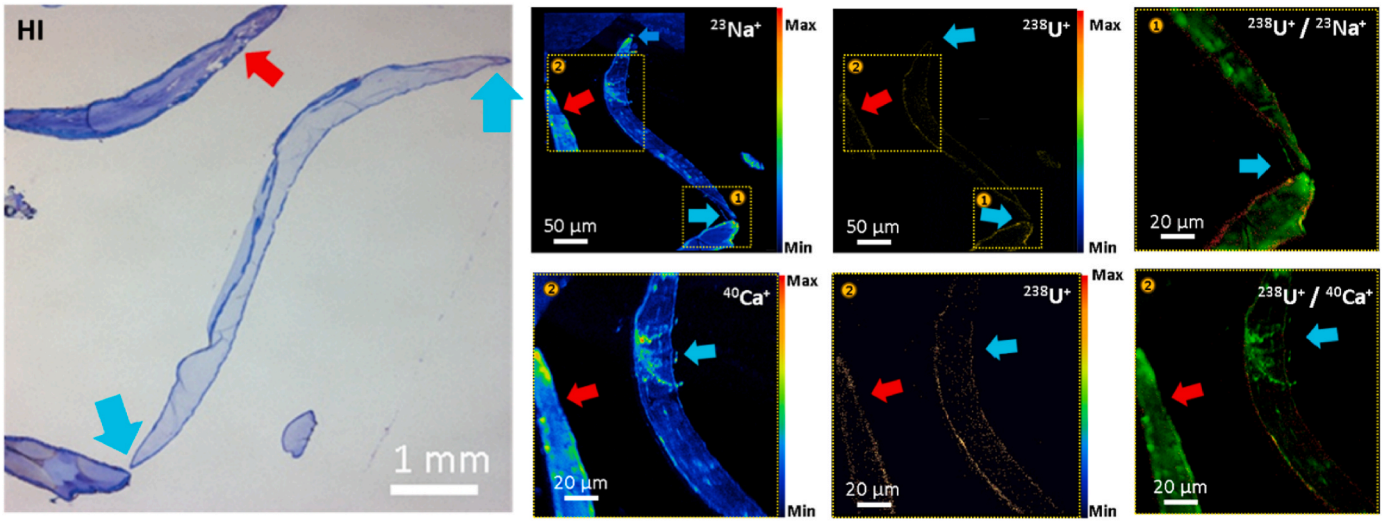

Fig. 6. HI: histological image of the byssus (*ex vivo*). Ionic (SIMS) images of $^{23}Na^+$, $^{40}Ca^+$, $^{238}U^+$ and overlay $^{238}U^+/^{23}Na^+$; $^{238}U^+/^{40}Ca^+$ of byssus contaminated *ex vivo* in doped in seawater with [U] = 10^{-3} M during 12 days. Red and blue arrows help identify and differentiate byssus. Yellow squares (1) and (2) marked the areas with uranium in the cuticle and diffused uranium in the matrix.

carbonate functions, oxygens + phosphorous (O + P) that mimic organophosphate functions, oxygens + sulfur (O + S) that mimic the presence of oxygens and thiolate functions (see Table 1). The O + C hypothesis did not lead to a satisfactory fit as shown in Fig. S11 of SI (agreement factor R = 4.4 %), whatever the distances. The O + P hypothesis did yield a satisfactory fit with U-O_{eq} distances equal to 2.26 Å and U···P distances equal to 3.31 Å (agreement factor R = 0.9 %). Finally, the O + S hypothesis did also yield a satisfactory fit with U-O_{eq} distances equal to 2.31 Å and U···S distances equal to 2.83 Å (agreement factor R = 1.0 %). Typical U ….P distances in previous examples of phosphorylated proteins or peptides are around 3.8–3.9 Å (for monodentate phosphate), much larger than the distance provided by this fit (Kumar et al., 2019; Safi et al., 2013; Starck et al., 2017). On the contrary, the U···S distance is in agreement with the distance provided for instance in the crystal structure of uranyl di (S-2,6-$Cl_2C_6H_3$) thiolate complex (average 2.72 Å) (Kannan et al., 2005). Also, the number of O + S atoms was fixed after several trials to have a total of 4 O + 2 S (=6) atoms on the equatorial plane of the uranyl complex (typical 2 + 6 coordination of uranyl). Therefore, it appears likely that thiol functions participate in the uranyl coordination sphere, although there are only scarce examples of uranyl-thiolate complexes. This assumption must be considered with much care although this finding would be in keeping with the role of metallothionein in metallic complexation in the hepatopancreas as discussed below.

To complement the information on uranium speciation in hepatopancreas, TRLIF data were recorded. Despite being a more sensitive probe than XAS, the contamination concentrations of [U] = 5.10^{-5} M were kept identical to those used for EXAFS to ensure a proper comparison of the data. Data presented in fluorescence show the presence of species with a very short lifetime (<500 ns) located between 330 nm and 470 nm, which corresponds to fluorescent organic species present in the biological matrix (Fig. S12 and Table S3 of SI). Maximum uranium wavelengths are positioned at 502-520-544-571 nm (delay time of 500 ns). A slight bathochromic shift between the maximum peaks at a time delay of 500 ns and at a time delay of 100 µs is observed indicating the presence of at least two species with different lifetimes and wavelengths in the hepatopancreas. To confirm this hypothesis, the lifetime (τ) was calculated using a simple formula: $I(t) = I_0 e^{-\frac{\Delta t}{\tau}}$.

Where I is the intensity at time t; I_0 the laser intensity, Δt delay time, τ lifetime of the species.

The adjustment with a single lifetime could not reproduce the curve and two significantly different lifetime parameters τ_1 = 0.7 µs and τ_2 = 53 µs had to be introduced (Fig. S13 of SI). Several uranyl species have been characterized in the literature with various ligands and counterions. By comparing the values of lifetimes and wavelengths with literature data, no obvious match could be found. However, data from the literature are mainly restricted to inorganic references (hydroxo, carbonato, and phosphato forms of uranyl) and only a few examples of coordination complexes with biomolecules are available, and none with thiol functions. Despite this limitation, the absence of a clear match with literature backs by default the assumption of thiol ligation, although this is not proof. One can also assume that at least two different species are present in hepatopancreas.

4. Discussion and conclusion

4.1. Uranium accumulation trends

Accumulation of uranium by *M. galloprovincialis* has been quantified with the measurement of CF values. It shows a clear trend in the organs under our experimental conditions in the following order: hepatopancreas ≫ gill > body ≥ mantle > foot. According to several reports, including those carried out by the RINBIO (Andral and Tomasino, 2010) and Cartochim (Démoulin L., 2014) programs aimed at monitoring the water quality in the Mediterranean Sea. The presence of Pb and Hg is higher in mussels collected from the naval base of Toulon (e.g. in TNB "petite rade" Hg = 0.31 µg g^{-1}) compared to other collection points (Hg median = 0.14 µg g^{-1}). Moreover, the analysis of seawater itself shows significant pollution by heavy metals in the TNB, well above the national average and regulatory norms (UNEP/MED IG.22/28, 2016). It should also be noted that the mussels obtained from the TNB harbor are native individuals that have always been present in this location. The comparison between mussels from a contaminated site and those from an unpolluted area was conducted to exemplify the potential impact of pollution on uranium accumulation. Due to the specific characteristics of the polluted site, analyses (imaging/speciation) were performed exclusively on mussels from the uncontaminated zone. Indeed, this site provides general conditions that can be extrapolated to sites with similar characteristics, namely those without contaminations. Although CF values for the entire mussel are comparable between TNB and VFM, hepatopancreas values show a significant increase for TNB *versus* VFM (a factor of 2). This difference in accumulation demonstrates that pollution of marine ecosystems has a direct impact on the bioaccumulation of uranium by mussels in a laboratory experiment. Furthermore, our

comparative study indicates that the presence of uranium in the hepatopancreas could reflect its storage by complexing molecules, the induction of which is more significant in areas polluted by heavy metals. Uranium could therefore be accumulated by the digestive gland through two mechanisms: transported between organs through the bloodstream and concentrated in the hepatopancreas, which possesses numerous proteins capable of binding heavy metals; and storage directly by digestive cells. However, at this stage of our study, the exact biochemical mechanisms are unknown. Previous studies have shown the adaptation capability of mussels when they are transferred from a non-polluted area to a polluted area (Damiens et al., 2007). Pollutants in seaport areas are diverse and may include heavy metals, PCBs, and PAHs. Their impact on mussels has been extensively studied. Mussels adapt to their environment and can increase certain biomarkers in response to the presence of pollutants in the water (e.g., Glutathione S-transferase, metallothionein, etc). Numerous metabolites can be analyzed as biomarkers to understand the impact of pollutants (e.g., DNA damage, and oxidative stress) (Cosson and Amiard, 1998; Damiens et al., 2007). Overall, our CF data are in very good agreement with this adaptation capability of mussels but also with the reported CF value (CF = 30) for uranium and mollusks by IAEA (IAEA, 2004). Two remarks need to be made at this point. First, mussels are members of the *Bivalvia* group, and extrapolation of the present results to all bivalves or mollusks should be considered with care. Second, adaptation of mussels to site pollution may be a complex phenomenon involving changes in the expression of certain metabolites. Establishing a causal relationship is beyond the scope of this work at this point, but a more detailed study will help to substantiate our observations.

The imaging and speciation results were obtained from mussels collected at VFM to collect information on the transfer of uranium to mussels in an unpolluted environment.

4.2. Uranium speciation in byssus

The first organ of interest is the byssus because it exhibits very high but scattered CF values during *in vivo* contamination. Images using μ-XRF and TEM obtained for byssus produced by mussels contaminated *in vivo* show homogeneous contamination of uranium at oxidation state + VI under the uranyl form (XANES spectra). The absence of visible dense aggregates in the tissue suggests that the uranyl is forming mainly (bio)molecular species and not condensed phases larger than the spatial resolution of the beam. SIMS images suggest that most of the uranyl is contained in the core of the thread. In contrast, SIMS images after *ex vivo* contamination show the presence of uranium mainly at the surface of the protective cuticle. This localization was not detected after *in vivo* contaminations, probably because of detection limits for *in vivo* samples, as the contamination concentration differs by a factor of 500. In the case of *in vivo* contamination, the presence of uranium in the core suggests an active mechanism that may be associated with uranium elimination. The mechanisms for metal excretion in the byssus are not well understood and may depend on the specific metal being studied (Hennebicq et al., 2013; Nicholson and Szefer, 2003). Several metals have been reported present in the byssal threads, such as Pb, Cu, Fe, and Zn. In the case of *ex vivo* contamination, a decreasing gradient concentration is observed from the cuticle to the core. The cuticle appears therefore capable of chelating uranyl but is also sufficiently permeable to diffuse uranium into the core. At the surface of the cuticle, the mpf-1 adhesive protein is known to have a strong affinity with metals (Harrington et al., 2018; Mesko et al., 2021; Sever et al., 2004). This protein is DOPA (3, 4-dihydroxyphenylalanine) rich, and can form metal complexes that contribute to the rigidity and hardness of the cuticle (McCartney, 2021; Priemel et al., 2020; Waite, 2017). The abundant presence of DOPA at the cuticle level could contribute to the formation of a stable complex with uranyl. The model used for the EXAFS adjustment is indeed based on a 1,2-dihydrobenzene that mimics the complexing site of the DOPA complex. This highlights the ability of biomaterials containing proteins rich in DOPA to chelate uranyl. This property could be used as a marker for the presence of uranyl contamination in the environment.

4.3. Uranium speciation in hepatopancreas

A second organ of interest for uranium accumulation is the hepatopancreas. This organ is designated in the mollusks as the main site of metal accumulation and storage. Moreover, the hepatopancreas is the most relevant organ for analyzing metallothionein which reflect the metal contamination and can store many metals such as Zn, Pb, Cd, and Cu (Coughtrey and Martin, 1976; Markich, 1998; Scholz, 1980; UNEP, 1999). Concentration of heavy metals in the hepatopancreas depends on several parameters such as time and, of course, speciation (Simon et al., 2011). The relationship between the bioaccumulation of metals and their toxicity is complex, as it depends on a perfect knowledge of the system and the speciation of the metal. The metal may be present in various forms (free ion, organic or inorganic complex) and interact with a biological membrane or the physiologically active sites of the organism. Therefore, the question of speciation addressed here is the essential first step for deciphering the toxicity mechanisms. In this study, images obtained with μ-XRF and TEM confirm the presence of diffuse uranium contamination inside the hepatopancreas. This is characterized by the homogeneous distribution of uranium at the given beam size resolution and, as in byssus, the absence of any condensed uranium phase in the organ. XANES and EXAFS spectra performed in imaging mode and bulk mode suggest the formation of a uranyl complex that incorporates oxygen and sulfur atoms in its coordination sphere. The presence of uranyl-thiolate interaction must be confirmed by protein extraction for instance. It is quite unusual for uranyl chemistry but may be explained here by the abundance of metallothionein in the organs. The occurrence of phosphate ligation is not totally incompatible with the EXAFS data but with a significant distortion of the phosphorous distances. This description of the speciation is qualitatively completed by the TRLIFS measurements (wavelength and lifetime) with values that do not correspond to species known in the literature.

In summary, our study aims to characterize the speciation of uranium in living organisms, which poses a significant challenge due to the low concentration of contaminants and the complexity of the marine environment. It is an attempt to decipher the mechanisms of contamination of bivalve *M. galloprovincialis* by uranium at oxidation state + VI. In this work, *M. galloprovincialis* was used as a model organism with contamination concentrations that tend to approach environmental relevance. The imaging and speciation results were obtained from mussels collected at VFM to collect information on the transfer of uranium to living organisms in an unpolluted environment. This information can be applied to numerous similar sites with or without specific pollution, providing a better understanding of the potential impact of uranium (more generally radionuclides) on living organisms. Speciation studies on living marine organisms are indeed challenging. They also do not address the biological process of uranium accumulation. But at this stage, they are an essential step for deciphering the bioaccumulation mechanisms of heavy radionuclides, such as uranium. Our methodology brings to light the speciation of uranium at different scales in two different organs, namely the byssus and the hepatopancreas, of a model organism. Due to the extremely large number of species in the marine ecosystem, the mechanisms of uranium accumulation are likely to vary. But this information is crucial for understanding the transfer of uranium from seawater to the marine biota and its potential impact on humans. Our method could be employed to better understand the uranium speciation in other model organisms and allow us to add complexity to the transfer models in the oceans.

CRediT authorship contribution statement

Romain Stefanelli: Writing – original draft, Methodology, Investigation. **Maria Rosa Beccia:** Validation, Methodology, Investigation.

Pier Lorenzo Solari: Investigation. **David Suhard:** Methodology, Investigation. **Sophie Pagnotta:** Investigation. **Aurélie Jeanson:** Conceptualization. **Jean Ulrich Mullot:** Investigation. **Françoise Vernier:** Investigation. **Christophe Moulin:** Investigation. **Marguerite Monfort:** Supervision. **Jean Aupiais:** Supervision. **Christophe Den Auwer:** Writing – review & editing, Supervision, Funding acquisition.

Declaration of competing interest

The authors declare the following financial interests/personal relationships which may be considered as potential competing interests:

DEN AUWER Christophe reports financial support was provided by French Alternative Energies and Atomic Energy Commission. If there are other authors, they declare that they have no known competing financial interests or personal relationships that could have appeared to influence the work reported in this paper.

Data availability

Data will be made available on request.

Acknowledgments

This work was financed by Commissariat à l'Energie Atomique et aux Energies Alternatives under the ESPERAME2 program. For Ionics images obtained on IMS -7FE7 the authors thank the PATERSON IRSN's mass spectrometry platform, contribution n∘20.

Appendix A. Supplementary data

Supplementary data to this article can be found online at https://doi.org/10.1016/j.envres.2024.118877.

References

Abney, C.W., Mayes, R.T., Saito, T., Dai, S., 2017. Materials for the recovery of uranium from seawater. Chem. Rev. 117, 13935–14013. https://doi.org/10.1021/acs.chemrev.7b00355.

Amiard, J.-C., Amiard-Triquet, C., Barka, S., Pellerin, J., Rainbow, P.S., 2006. Metallothioneins in aquatic invertebrates: their role in metal detoxification and their use as biomarkers. Aquat. Toxicol. 76, 160–202. https://doi.org/10.1016/j.aquatox.2005.08.015.

Andral, B., Tomasino, C., 2010. Evaluation de la qualité des eaux basée sur l'utilisation de stations artificielles de moules en Méditerranée : résultats de la campagne 2009 (No. RST.DOPLER/PAC/10-19). Ifremer.

Atwood, D.A. (Ed.), 2010. Radionuclides in the Environment, EIC Books. Wiley, Chichester.

Beneš, P., 1999. The environmental impacts of uranium mining and milling and the methods of their reduction. In: Choppin, G.R., Khankhasayev, M.Kh (Eds.), Chemical Separation Technologies and Related Methods of Nuclear Waste Management. Springer, Netherlands, Dordrecht, pp. 225–246. https://doi.org/10.1007/978-94-011-4546-6_13.

Beyer, J., Green, N.W., Brooks, S., Allan, I.J., Ruus, A., Gomes, T., Bråte, I.L.N., Schøyen, M., 2017. Blue mussels (Mytilus edulis spp.) as sentinel organisms in coastal pollution monitoring: a review. Mar. Environ. Res. 130, 338–365. https://doi.org/10.1016/j.marenvres.2017.07.024.

Bryan, G.W., Waldichuk, M., Pentreath, R.J., Darracott, Ann, 1979. Bioaccumulation of marine pollutants. Phil. Trans. Roy. Soc. Lond. B 286, 483–505. https://doi.org/10.1098/rstb.1979.0042.

Carpene, E., George, S.G., 1981. Absorption of cadmium by gills of Mytilus edulis. Mol. Physiol. 1, 23–34. https://doi.org/10.1016/0009-2797(79)90154-6.

Castrillejo, M., Witbaard, R., Casacuberta, N., Richardson, C.A., Dekker, R., Synal, H.-A., Christl, M., 2020. Unraveling 5 decades of anthropogenic 236U discharge from nuclear reprocessing plants. Sci. Total Environ. 717, 137094 https://doi.org/10.1016/j.scitotenv.2020.137094.

Cosson, R.P., Amiard, J.-C., 1998. Use of metallothioneins as biomarkers of exposure to metals. In: Use of Biomarkers for Environmental Quality Assessment. CRC Press.

Coughtrey, P.J., Martin, M.H., 1976. The distribution of Pb, Zn, Cd and Cu within the pulmonate mollusc Helix aspersa müller. Oecologia 23, 315–322. https://doi.org/10.1007/BF00345960.

Damiens, G., Gnassia-Barelli, M., Loquès, F., Roméo, M., Salbert, V., 2007. Integrated biomarker response index as a useful tool for environmental assessment evaluated using transplanted mussels. Chemosphere 66, 574–583. https://doi.org/10.1016/j.chemosphere.2006.05.032.

Démoulin, L., 2014. Cartographie de la contamination chimique des sédiments de la Rade de Toulon (No. RST.ODE/LER-PAC/14-10). Ifremer.

Eisenbud, M., Gesell, T., 1997. Environmental Radioactivity from Natural, Industrial and Military Sources, fourth ed.

Fisher, N.S., Teyssié, J.-L., Fowler, S.W., Wang, W.-X., 1996. Accumulation and retention of metals in mussels from food and water: a comparison under field and laboratory conditions. Environ. Sci. Technol. 30, 3232–3242. https://doi.org/10.1021/es960009u.

Gascoyne, M., 1992. Geochemistry of the Actinides and Their Daughters. Clarendon Press, United Kingdom.

Goldberg, E.D., Bertine, K.K., 2000. Beyond the Mussel Watch — new directions for monitoring marine pollution. Sci. Total Environ. 247, 165–174. https://doi.org/10.1016/S0048-9697(99)00488-X.

Gorden, A.E.V., Xu, J., Raymond, K.N., Durbin, P., 2003. Rational design of sequestering agents for plutonium and other actinides. Chem. Rev. 103, 4207–4282. https://doi.org/10.1021/cr990114x.

Harrington, M.J., Jehle, F., Priemel, T., 2018. Mussel byssus structure-function and fabrication as inspiration for biotechnological production of advanced materials. Biotechnol. J. 13, 1800133 https://doi.org/10.1002/biot.201800133.

Hédouin, L., Metian, M., Teyssié, J.-L., Fowler, S.W., Fichez, R., Warnau, M., 2006. Allometric relationships in the bioconcentration of heavy metals by the edible tropical clam Gafrarium tumidum. Sci. Total Environ. 366, 154–163. https://doi.org/10.1016/j.scitotenv.2005.10.022.

Hennebicq, R., Fabra, G., Pellerin, C., Marcotte, I., Myrand, B., Tremblay, R., 2013. The effect of spawning of cultured mussels (Mytilus edulis) on mechanical properties, chemical and biochemical composition of byssal threads. J. Aquac. 410–411, 11–17. https://doi.org/10.1016/j.aquaculture.2013.06.011.

IAEA, 1973. Radioactive contamination of the marine environment. Proceedings Series of an International conference Seattle, july 1972. International Atomic Energy Agency, Vienna.

IAEA, 2004. Sediment distribution coefficients and concentration factors for biota in the marine environment. Technical reports series. Vienna. International Atomic Energy Agency.

Jeng, M.-S., Jeng, W.-L., Hung, T.-C., Yeh, C.-Y., Tseng, R.-J., Meng, P.-J., Han, B.-C., 2000. Mussel Watch: a review of Cu and other metals in various marine organisms in Taiwan, 1991–98. Environ. Pollut. 110, 207–215. https://doi.org/10.1016/S0269-7491(99)00304-8.

Kägi, J.H.R., Kojima, Y., 1987. Chemistry and biochemistry of metallothionein. In: Kägi, Jeremias H.R., Kojima, Yutaka, Metallothionein, I.I. (Eds.), Experientia Supplementum. Birkhäuser Basel, Basel, pp. 25–61. https://doi.org/10.1007/978-3-0348-6784-9_3.

Kannan, S., Barnes, C.L., Duval, P.B., 2005. Synthesis and structural characterization of a uranyl(VI) complex possessing unsupported unidentate thiolate ligands. Inorg. Chem. 44, 9137–9139. https://doi.org/10.1021/ic0517117.

Klerks, P.L., Bartholomew, P.R., 1991. Cadmium accumulation and detoxification in a Cd-resistant population of the oligochaete Limnodrilus hoffmeisteri. Aquat. Toxicol. 19, 97–112. https://doi.org/10.1016/0166-445X(91)90030-D.

Konstantinou, M., Pashalidis, I., 2004. Speciation and spectrophotometric determination of uranium in seawater. Mediterr. Mar. Sci. 5, 55. https://doi.org/10.12681/mms.210.

Kumar, S., Creff, G., Hennig, C., Rossberg, A., Steudtner, R., Raff, J., Vidaud, C., Oberhaensli, F.R., Bottein, M.D., Den Auwer, C., 2019. How do actinyls interact with hyperphosphorylated yolk protein phosvitin? Chem. Eur J. 25, 12332–12341. https://doi.org/10.1002/chem.201902015.

Lambert, I.B., Heier, K.S., 1968. Estimates of the crustal abundances of thorium, uranium and potassium. Chem. Geol. 3, 233–238. https://doi.org/10.1016/0009-2541(68)90030-2.

Li, Y., Yang, H., Liu, N., Luo, J., Wang, Q., Wang, L., 2015. Cadmium accumulation and metallothionein biosynthesis in cadmium-treated freshwater mussel anodonta woodiana. PLoS One 10, e0117037. https://doi.org/10.1371/journal.pone.0117037.

Liang, L.N., He, B., Jiang, G.B., Chen, D.Y., Yao, Z.W., 2004. Evaluation of mollusks as biomonitors to investigate heavy metal contaminations along the Chinese Bohai Sea. Sci. Total Environ. 324, 105–113. https://doi.org/10.1016/j.scitotenv.2003.10.021.

Lin, M., Qiao, J., Hou, X., Dellwig, O., Steier, P., Hain, K., Golser, R., Zhu, L., 2021. 70-Year anthropogenic uranium imprints of nuclear activities in baltic sea sediments. Environ. Sci. Technol. 55, 8918–8927. https://doi.org/10.1021/acs.est.1c02136.

Lorens, I., Solari, P.L., Sitaud, B., Bes, R., Cammelli, S., Hermange, H., Othmane, G., Safi, S., Moisy, P., Wahu, S., Bresson, C., Schlegel, M.L., Menut, D., Bechade, J.-L., Martin, P., Hazemann, J.-L., Proux, O., Auwer, C.D., 2014. X-ray absorption spectroscopy investigations on radioactive matter using MARS beamline at SOLEIL synchrotron: radiochim. Acta 102, 957–972. https://doi.org/10.1515/ract-2013-2241.

Machado, J., Lopes-Lima, M., 2011. Calcification mechanism in freshwater mussels: potential targets for cadmium. Toxicol. Environ. Chem. 93, 1778–1787. https://doi.org/10.1080/02772248.2010.503656.

Maloubier, M., Solari, P.L., Moisy, P., Monfort, M., Den Auwer, C., Moulin, C., 2015. XAS and TRLIF spectroscopy of uranium and neptunium in seawater. Dalton Trans. 44, 5417–5427. https://doi.org/10.1039/C4DT03547J.

Marigómez, I., Soto, M., Cajaraville, M.P., Angulo, E., Giamberini, L., 2002. Cellular and subcellular distribution of metals in molluscs. Microsc. Res. Tech. 56, 358–392. https://doi.org/10.1002/jemt.10040.

Markich, S.J., 1998. Effects of Biological and Physicochemical Variables on the Valve Movement Responses of Freshwater Bivalves to Manganese, Uranium,cadmium and Copper (Thesis).

McCartney, M.A., 2021. Structure, function and parallel evolution of the bivalve byssus, with insights from proteomes and the zebra mussel genome. Phil. Trans. R. Soc. B 376, 20200155. https://doi.org/10.1098/rstb.2020.0155.

Mesko, M., Xiang, L., Bohle, S., Hwang, D.S., Zeng, H., Harrington, M.J., 2021. Catechol-vanadium binding enhances cross-linking and mechanics of a mussel byssus coating protein. Chem. Mater. 33, 6530–6540. https://doi.org/10.1021/acs.chemmater.1c02063.

Morris, K., Raiswell, R., 2002. Chapter 4 Biogeochemical cycles and remobilisation of the actinide elements. In: Keith-Roach, M.J., Livens, F.R. (Eds.), Radioactivity in the Environment, Interactions of Microorganisms with Radionuclides. Elsevier, pp. 101–141. https://doi.org/10.1016/S1569-4860(02)80033-X.

Mossand, G., Lelong, E., Xing, C., Ndebulia Watchou, F., Leydier, A., Arrachart, G., Pellet-Rostaing, S., 2023. Bis-catecholamide-based materials for uranium extraction. ChemPlusChem 88, e202200412. https://doi.org/10.1002/cplu.202200412.

Moulin, C., Laszak, I., Moulin, V., Tondre, C., 1998. Time-Resolved laser-induced fluorescence as a unique tool for low-level uranium speciation. Appl. Spectrosc. 52, 528–535. https://doi.org/10.1366/0003702981944076.

Nicholson, S., Szefer, P., 2003. Accumulation of metals in the soft tissues, byssus and shell of the mytilid mussel Perna viridis (Bivalvia: mytilidae) from polluted and uncontaminated locations in Hong Kong coastal waters. Mar. Pollut. Bull. 46, 1040–1043. https://doi.org/10.1016/S0025-326X(03)00152-8.

OSPAR, 2018. CEMP Guidelines for Monitoring Contaminants in Biota (No. Agreement 1999-02) (OSPAR).

Priemel, T., Palia, R., Babych, M., Thibodeaux, C.J., Bourgault, S., Harrington, M.J., 2020. Compartmentalized processing of catechols during mussel byssus fabrication determines the destiny of DOPA. Proc. Natl. Acad. Sci. USA 117, 7613–7621. https://doi.org/10.1073/pnas.1919712117.

Rainbow, P.S., 1995. Biomonitoring of heavy metal availability in the marine environment. Mar. Pollut. Bull. 31, 183–192. https://doi.org/10.1016/0025-326X(95)00116-5.

Safi, S., Creff, G., Jeanson, A., Qi, L., Basset, C., Roques, J., Solari, P.L., Simoni, E., Vidaud, C., Den Auwer, C., 2013. Osteopontin: a uranium phosphorylated binding-site characterization. Chem. Eur J. 19, 11261–11269. https://doi.org/10.1002/chem.201300989.

Sakaguchi, A., Kawai, K., Steier, P., Quinto, F., Mino, K., Tomita, J., Hoshi, M., Whitehead, N., Yamamoto, M., 2009. First results on 236U levels in global fallout. Sci. Total Environ. 407, 4238–4242. https://doi.org/10.1016/j.scitotenv.2009.01.058.

Sandalls, F.J., Segal, M.G., Victorova, N., 1993. Hot particles from Chernobyl: a review. J. Environ. Radioact. 18, 5–22. https://doi.org/10.1016/0265-931X(93)90063-D.

Scholz, N., 1980. Accumulation, loss and molecular distribution of cadmium in Mytilus edulis. Helgol. Meeresunters. 33, 68–78. https://doi.org/10.1007/BF02414736.

Sever, M.J., Weisser, J.T., Monahan, J., Srinivasan, S., Wilker, J.J., 2004. Metal-mediated cross-linking in the generation of a marine-mussel adhesive. Angew. Chem. Int. Ed. 43, 448–450. https://doi.org/10.1002/anie.200352759.

Simon, O., Floriani, M., Cavalie, I., Camilleri, V., Adam, C., Gilbin, R., Garnier-Laplace, J., 2011. Internal distribution of uranium and associated genotoxic damages in the chronically exposed bivalve Corbicula fluminea. J. Environ. Radioact. 102, 766–773. https://doi.org/10.1016/j.jenvrad.2011.04.004.

Sitaud, B., Solari, P.L., Schlutig, S., Llorens, I., Hermange, H., 2012. Characterization of radioactive materials using the MARS beamline at the synchrotron SOLEIL. J. Nucl. Mater., Microstructure Properties of Irradiated Materials 425, 238–243. https://doi.org/10.1016/j.jnucmat.2011.08.017.

Solé, V.A., Papillon, E., Cotte, M., Walter, Ph, Susini, J., 2007. A multiplatform code for the analysis of energy-dispersive X-ray fluorescence spectra. Spectrochim. Acta B: At. Spectrosc. 62, 63–68. https://doi.org/10.1016/j.sab.2006.12.002.

Starck, M., Laporte, F.A., Oros, S., Sisommay, N., Gathu, V., Solari, P.L., Creff, G., Roques, J., Den Auwer, C., Lebrun, C., Delangle, P., 2017. Cyclic phosphopeptides to rationalize the role of phosphoamino acids in uranyl binding to biological targets. Chem. Eur J. 23, 5281–5290. https://doi.org/10.1002/chem.201605481.

Szigethy, G., Raymond, K.N., 2011. Hexadentate terephthalamide(bis-hydroxypyridinone) ligands for uranyl chelation: structural and thermodynamic consequences of ligand variation. J. Am. Chem. Soc. 133, 7942–7956. https://doi.org/10.1021/ja201511u.

Topin, S., Aupiais, J., 2016. The pentavalent actinide solution chemistry in the environment. J. Environ. Radioact. 153, 237–244. https://doi.org/10.1016/j.jenvrad.2015.12.016.

Torres, F.G., Troncoso, O.P., Torres, C.E., 2012. Chapter 14. Mussel byssus fibres: a tough biopolymer. In: John, M.J., Thomas, S. (Eds.), Green Chemistry Series. Royal Society of Chemistry, Cambridge, pp. 305–329. https://doi.org/10.1039/9781849735193-00305.

UNEP, 1999. In: Manual on the Biomarkers Recommended for the Med Pol Biomonitoring Programme. United Nations Environment Programme, Athens.

UNEP/MED IG.22/28, 2016. Integrated Monitoring and Assessment Programme of the Mediterranean Sea and Coast and Related Assessment Criteria.

UNEPMAP, 2023. https://www.unep.org/unepmap/fr, 7.27.23.

UNSCEAR, 2015. Sources, Effects and Risks of Ionizing Radiation, United Nations Scientific Committee on the Effects of Atomic Radiation (UNSCEAR) 2012 Report, United Nations Scientific Committee on the Effects of Atomic Radiation (UNSCEAR) Reports. UN. https://doi.org/10.18356/2ed43f39-en. United Nations Scientific Committee on the Effects of Atomic Radiation.

Viarengo, A., Nott, J.A., 1993. Mechanisms of heavy metal cation homeostasis in marine invertebrates. Comp. Biochem. Physiol., Part C: Toxicol. Pharmacol. 104, 355–372. https://doi.org/10.1016/0742-8413(93)90001-2.

Viarengo, A., Burlando, B., Cavaletto, M., Marchi, B., Ponzano, E., Blasco, J., 1999. Role of metallothionein against oxidative stress in the mussel *Mytilus galloprovincialis*. Am. J. Physiol. Regul. Integr. Comp. Physiol. 277, R1612–R1619. https://doi.org/10.1152/ajpregu.1999.277.6.R1612.

Waite, J.H., 2017. Mussel adhesion – essential footwork. J. Exp. Biol. 220, 517–530. https://doi.org/10.1242/jeb.134056.

Wallace, W., Luoma, S., 2003. Subcellular compartmentalization of Cd and Zn in two bivalves. II. Significance of trophically available metal (TAM). Mar. Ecol. Prog. Ser. 257, 125–137. https://doi.org/10.3354/meps257125.

Wang, W.-X., Fisher, N.S., 1999. Effects of calcium and metabolic inhibitors on trace element uptake in two marine bivalves. J. Exp. Mar. Biol. Ecol. 236, 149–164. https://doi.org/10.1016/S0022-0981(98)00195-6.

Wang, W., Fisher, N., Luoma, S., 1996. Kinetic determinations of trace element bioaccumulation in the mussel Mytilus edulis. Mar. Ecol. Prog. Ser. 140, 91–113. https://doi.org/10.3354/meps140091.

Widdows, J., Donkin, P., 1992. Mussels and environmental contaminants : bioaccumulation and physiological aspects. Dev. Aquacult. Fish. Sci. 25, 383–424.

Winkler, S.R., Steier, P., Carilli, J., 2012. Bomb fall-out 236U as a global oceanic tracer using an annually resolved coral core. Earth Planet Sci. Lett. 359–360, 124–130. https://doi.org/10.1016/j.epsl.2012.10.004.

Wu, F., Pu, N., Ye, G., Sun, T., Wang, Z., Song, Y., Wang, W., Huo, X., Lu, Y., Chen, J., 2017. Performance and mechanism of uranium adsorption from seawater to poly (dopamine)-inspired sorbents. Environ. Sci. Technol. 51, 4606–4614. https://doi.org/10.1021/acs.est.7b00470.